

ORIGINAL ARTICLE

Conversion of selenite by *Haloferax alexandrinus* GUSF-1 (KF796625) to pentagonal selenium nanoforms which in vitro modulates the formation of calcium oxalate crystals

Jyothi J. Alvares | Irene J. Furtado 

Department of Microbiology, Goa University, Taleigao, India

CorrespondenceProf. Irene J. Furtado, Department of Microbiology, Goa University, Taleigao Plateau, Goa 403206, India.
Email: ijfurtado@unigoa.ac.in**Abstract**

Aim: To investigate the ability of *Haloferax alexandrinus* GUSF-1 (KF796625) to biosynthesize non-toxic elemental selenium (Se^0) and check their capacity in in vitro crystal structure modulation of calcium oxalate, which are implicated in the development of renal calculi.

Methods and Results: *Haloferax alexandrinus* GUSF-1 (KF796625) during growth in the presence of 5 mmol L^{-1} of selenite formed insoluble brick-red particles. Se^0 formed was monitored spectrophotometrically using a combination of two assays; the ascorbic acid reduction and sodium sulphide solubilization assay. After 168 h of growth, 2.89 mmol L^{-1} of Se^0 was formed from 4.9 mmol L^{-1} of selenite. Absorption bands at 1.5, 11.2 and 12.5 keV in EDX spectroscopy confirmed that the brick-red particulate matter was Se^0 . Furthermore, these selenium nanoparticles (SeNPs) were pentagonal in shape in transmission electron microscopy imaging. The peak positions in X-ray diffractogram at 2θ values of 23.40° , 29.66° , 41.26° , 43.68° , 45.24° , 51.62° , 55.93° and 61.47° and the relative intensities further confirmed the formation of Se^0 . In vitro addition of 50 and $100 \mu\text{g ml}^{-1}$ of these SeNPs to the mixture of sodium chloride, calcium chloride and sodium oxalate affected and modulated the shape and size of rectangular-shaped calcium oxalate crystals (average area of $1.23 \pm 0.2 \mu\text{m}^2$) to smaller rectangular-shaped crystals (average area of $0.54 \pm 0.2 \mu\text{m}^2$) and spherical-shaped crystals (average area $0.13 \pm 0.005 \mu\text{m}^2$).

Conclusion: *Haloferax alexandrinus* GUSF-1 (KF796625) transformed selenite to Se^0 pentagonal nanoforms that modulated in vitro the formation of crystal shape and size of calcium oxalate.

Significance and Impact of Study: There are no reports on conversion of selenite to Se^0 among the *Haloferax* genera, and this study involving the formation of pentagonal SeNPs with capacity to modulate the formation of calcium oxalate crystals in haloarchaea is recorded as the first report and of significance in pharmaceutical research related to formulations abetting urinary calculi.

KEYWORDScalcium oxalate crystals, *Haloferax alexandrinus* GUSF-1 (KF796625), modulation, selenite, selenium nanoparticles

The authors dedicate this publication to all Goans on the diamond jubilee year of liberation of the State of Goa.

INTRODUCTION

Selenium is an essential element for life and is released into the environment through either anthropogenic sources of industrial and agricultural activities or from weathering of selenium-rich rocks (Wen & Carignan, 2007). It exists in the environment as inorganic oxyanions, including ionic selenate (SeO_4^{2-} , Se^{6+}), selenite (SeO_3^{2-} , Se^{4+}), solid-state selenium (Se^0) and selenocysteine/selenoproteins (Papp et al., 2007). Oxyanions of selenite (SeO_3^{2-}) and selenate (SeO_4^{2-}) are the most toxic forms of selenium because of their solubility and bioavailability. The recommended tolerable upper intake level for adults is set at $400 \mu\text{g day}^{-1}$ based on their adverse effects causing selenosis (Institute of Medicine (US) Panel on Dietary Antioxidants and Related Compounds, 2000). On the other hand, elemental selenium at $40 \mu\text{g day}^{-1}$ is recommended by the World Health Organization (WHO) as the adequate dietary requirement, because selenium forms an essential element in humans who have selenoproteins and enzymes containing selenocysteine (Zhang & Spallholz, 2011).

Microorganisms play a crucial role in transforming different selenium oxyanions through metabolic reactions under aerobic or anaerobic conditions to Se^0 (Wadhvani et al., 2016). Often, the reduction of selenite results in the precipitation of insoluble products that ultimately accumulate within the cell or in extracellular environment (Debieux et al., 2011). Reduction of selenium oxyanions to SeNPs is reported across domains; using plants (Sharma et al., 2014), filamentous, polymorphic and unicellular fungi (Gharieb et al., 1995), actinomycete bacteria (Forootanfar et al., 2013) and among bacterial genera such as *Thauera selenatis* (Macy et al., 1993), *Enterobacter cloacae* SLD1a-1 (Losi & Frankenberger, 1997), *Rhodospirillum rubrum* (Kessi et al., 1999), *Rhodobacter sphaeroides* (Bebien et al., 2001), *Shewanella oneidensis MR-1* (Klonowska et al., 2005). Sparse reports among haloarchaea from the archaeal domain are also available; *Halorubrum xinjiangense* (Güven et al., 2013) isolated from Tuz (Salt) lake brine, *Halococcus salifonidae* BK18 from a solar saltern of Goa (Srivastava et al., 2014) and *Halogeometricum* sp. E118, an isolate from the crystallizer ponds of the Tis solar saltern (Abdollahnia et al., 2020) are known to produce SeNPs. In microbes, selenite to insoluble Se^0 is known to be catalysed predominantly by the enzyme nitrate reductase (DeMoll-Decker & Macy, 1993; Srivastava et al., 2014). Selenite is also reduced to Se^0 in abiotic reactions with reduced thiols such as glutathione and in the presence of glutathione reductase (Ganther, 1971; Kessi & Hanselmann, 2004).

SeNPs are also reported for their importance in medical applications due to their different properties such as

enhanced biocompatibility (Barnaby et al., 2011), photoconductive (Luo et al., 2009), antiproliferative (Srivastava et al., 2014), antigenotoxic (Prasad & Selvaraj, 2014) and their ability to modulate the shape of calcium oxalate crystals (Liang et al., 2009; Zhong et al., 2015). In recent times, nanoselenium has also been reported to exhibit lower toxicity in humans than its inorganic or organic form (Zhang & Spallholz, 2011), possibly because of its good antioxidant properties (Prasad et al., 2013).

The formation of large renal calculi consisting of calcium oxalate is favoured under physiological pH in humans (Lieske et al., 1999). These crystals accumulate in the renal system, interact with the renal epithelium and cause or induce oxidative damage resulting in cell death and damage to nearby cells (Lulich et al., 2012). Hence, there is a growing search for molecules with antioxidant properties. Gallic acid-chitosan conjugates with antioxidant properties although preferred as molecules to combat the oxidative stress induced during the formation of renal calculi are costly (Queiroz et al., 2019).

Haloferax alexandrinus (*Hfx. alexandrinus*) GUSF-1 (KF796625), during its growth in 20% mineral medium in the presence of manganese chloride is reported to produce rhodochrosite (Naik & Furtado, 2019); Ag^0 with silver nitrate in 25% NaCl-tryptone-yeast extract (NTYE) (Patil et al., 2014) and Te^0 with potassium tellurite (Alvares & Furtado, 2021b). Because of these features and the ability to produce multiple antioxidants primarily comprising of bacterioruberin (Alvares & Furtado, 2018, 2021a, 2021c), we chose the culture to investigate its ability to biosynthesize SeNPs from selenite during growth. Furthermore, the pentagonal-shaped SeNPs were successfully used in vitro to modulate the formation of shape and size of calcium oxalate crystals.

MATERIALS AND METHODS

Chemicals and reagents

All chemicals and reagents used were of analytical grade (Himedia laboratories, India). A stock solution of 100 mmol L^{-1} selenite was prepared by dissolving sodium selenite in ultra-pure water (Millipore, Direct Q-3).

Culture and maintenance

Hfx. alexandrinus GUSF-1 (GenBank accession number KF796625), a haloarchaeon isolate from a salt sample of a solar saltern in Goa-India (Sequeira, 1992) was routinely cultured and maintained at ambient room temperature (RT; 28–32°C) on agar slopes of NTYE medium, which

consists of $\text{MgSO}_4 \cdot 7 \text{H}_2\text{O}$ (20 g L^{-1}), KCl (5 g L^{-1}), $\text{CaCl}_2 \cdot 2 \text{H}_2\text{O}$ (0.2 g L^{-1}), tryptone (5 g L^{-1}), yeast extract (3 g L^{-1}) and NaCl (250 g L^{-1}) at pH 7 (Raghavan & Furtado, 2004).

Growth of *Hfx. alexandrinus* GUSF-1 in the presence of selenite

The culture was pre-grown in NTYE at 37°C to reach its log-phase and then used to inoculate NTYE containing filter-sterilized 5 mmol L^{-1} selenite. The flasks were then incubated at 150 rpm at 37°C on an orbital shaker (REMI CIS-24 PLUS, India). Growth of culture was monitored regularly as colony-forming units (CFUs), for which an aliquot of 100 μl of cells, growing in the presence of selenite was aseptically withdrawn at regular intervals, spread onto NTYE agar, incubated at 37°C and was expressed in terms of CFUs. Control plates with NTYE agar were also maintained. At the end of incubation (7 days), cells were harvested by centrifuging a litre of culture broth at 8000 rpm, 4°C, for 10 min (Eppendorf centrifuge 5417 R, Germany). The pellet was washed with sterile 15% NaCl (w v^{-1}). The cellular pigment was monitored and extraction was carried out according to Gaonkar and Furtado (2018). The cell-free acetone extract was recovered by centrifuging with minimum exposure to light and scanned from 300 to 600 nm using a UV-Vis dual-beam spectrophotometer (Shimadzu-UV 1601, Japan) against acetone as a reference solution.

Estimation of selenite using ascorbic acid reduction

Cell-free culture supernatant, which was pre-filtered through 0.22- μm nitrocellulose membrane (MF-Millipore™), and 50 mM aqueous ascorbic acid were mixed in a 1:4 (v v^{-1}), and selenium formed was estimated as described by Malhotra et al. (2014).

Estimation of Se^0 by sodium sulphide solubilization

Elemental selenium was estimated by solubilizing it in 1 M sodium sulphide (Biswas et al., 2011). The orange-red material formed from selenite reduction by ascorbic acid was separated by centrifugation (10,000 rpm, 4°C, 30 min). The pellet was re-dissolved in 1 ml of 1 M Na_2S for 1 h and centrifuged (10,000 rpm, 4°C, 10 min) to remove debris. The red-brown supernatant was spectrophotometrically monitored at 500 nm with 1 M Na_2S solution as the reference solution. Monitoring and deduction of the

residual selenite and Se^0 formed during growth of culture was achieved using the above two methods serially (i) by reducing different concentrations of selenite solution (for residual selenite and Se^0) with ascorbic acid and (ii) solubilizing the Se^0 formed with 1 M Na_2S . The linear part of the curve between 0 and 5 mmol L^{-1} selenite was used for deducing the concentrations. Standard deviation was calculated for triplicate samples.

Localization of selenite reducing activity in *Hfx. alexandrinus* GUSF-1

Preparation of extracellular polymeric substance (EPS) was carried out according to a previously described method (Del Gallo & Haegi, 1990) by mixing filtered cell-free supernatant (CFS) obtained from a seventh day grown culture broth, with an equal volume of cold ethanol at -20°C and allowed to stand overnight at the same temperature. The EPS pellet was collected by centrifuging the overnight precipitated mixture (10,000 rpm, 4°C, 30 min) and dispersed in 15% NaCl (w v^{-1}). The soluble protein (SP) and membrane fraction (MF) from wet cells of *Hfx. alexandrinus* GUSF-1 was obtained from cells grown in NTYE for 7 days. Cell mass collected from the culture broth was then washed thrice with 15% NaCl (w v^{-1}). Wet cells (100 mg) were then suspended in 5 ml of distilled water, centrifuged (10,000 rpm, 4°C, 10 min) to obtain the SP, which was used instantly and the pellet on dispersal in 15% NaCl (w v^{-1}) was used as the MF. All fractions, CFS, EPS, SP and MF were tested for their ability to form Se^0 from selenite. The total protein content of SP was determined using the Lowry method (Lowry et al., 1951).

Assay of selenium formation from selenite

To each well of a 96-well micro-titre plate was added 100 μl of CFS/EPS/SP/MF along with 10 μl of 5 mmol L^{-1} selenite, 88 μl of McIlvaine buffer (containing 15% NaCl) of pH 6 & 7 and 2 μl of NADH. Wells with no selenite and without CFS/EPS/SP/MF were also maintained. Plates were left at RT and monitored for formation of red colour according to Lampis et al. (2014).

Effect of sodium arsenite and sodium azide on selenium formation

Sodium arsenite at 0.01, 0.05 and 0.1 mmol L^{-1} and sodium azide at 5 and 10 mmol L^{-1} were added to separate wells containing 100 μl of either CFS or SP or MF, 10 μl

of 5 mmol L⁻¹ selenite, 80 µl of McIlvaine buffer, 2 µl of NADH and the final volume was adjusted with the buffer. Wells with no inhibitor, no selenite and without CFS/SP/MF were also maintained. The effect of the inhibitors on selenium formation was assessed.

Fourier transform infrared analysis

At the end of 7 days of incubation, growing cells with the brick-red particulate matter were harvested from the culture broth by centrifuging (10,000 rpm, 4°C, 40 min), washed with 15% NaCl (w v⁻¹), dried at 80°C (BIOTECHNICS, India) and ground to a very fine powder in an agate mortar and pestle. Infrared spectroscopic measurements were obtained by mixing the sample with KBr powder in a 1:10 ratio (w w⁻¹). The KBr pellet was then analysed in the range of 4000–400 cm⁻¹ at a resolution of 4 cm⁻¹, using a Fourier transform infrared (FT-IR) spectrometer (IRPrestige-21 Shimadzu). In addition, the FT-IR spectrum of the cells growing in NTYE medium devoid of selenite was also obtained. The spectra obtained were checked for the presence of functional group peaks.

Release and recovery of nanomaterial

Harvested and washed cells (10 g) with the brick-red particulate material were suspended in ultrapure water in a sterile conical flask and kept overnight on the orbital shaker at 150 rpm. The released brick-red material was recovered by centrifuging (10,000 rpm, 4°C, 40 min), transferred to a Petri-plate, dried at 80°C, pulverized and used for characterization.

Scanning electron microscopy and energy-dispersive X-ray spectroscopy analysis

To observe the association of *Hfx. alexandrinus* GUSF-1 with selenite, the culture growing in NTYE containing 5 mmol L⁻¹ selenite was centrifuged after 7 days of growth (10,000 rpm, 4°C, 15 min) and washed with 15% NaCl to remove medium impurities. Thin smear of these cells was prepared on a clean glass coverslip (2 × 2 cm), air-dried and exposed to 2.0% (v/v) glutaraldehyde in 20% NaCl, at RT overnight. Coverslip was exposed to an increasing gradient of acetone: water of 30%, 50%, 70% and 90% for 10 min each and finally to 100% acetone. Coverslip was then coated with gold and mounted on to the copper stub and observed under SEM equipped with

energy-dispersive X-ray spectroscopy (EDX) (JEOL JSM-5800LV, Japan).

Furthermore, to determine the chemical composition of the brick-red material, the dried fine powder was placed on the copper stub as a very thin layer, coated with gold using a high vacuum evaporator and mounted on a sample holder approximately 50 mm from the bottom of the sputter head. This was then analysed using JEOL JSM-5800LV scanning and EDX spectroscope, Japan.

Characterization of SeNPs

Ultraviolet-visible and Raman spectrophotometric analysis

Finely ground sample was suspended in methanol and sonicated (Labsonic M, B. Braun Biotech International, Germany) for 2 min for uniform dispersion of the nanomaterial. The resulting mixture was scanned in the spectrophotometer in the UV-visible region against methanol as the reference solution. The confocal Raman spectrum of the finely ground sample powder was recorded using an STR 500 confocal micro Raman spectrometer (AIRIX Corp—x20, Japan).

X-ray diffraction analysis

The X-ray diffraction (XRD) measurements was carried out using a Rigaku Miniflex X-ray diffractometer, USA and scanned in the 2θ range of 30–80° at a voltage of 40 kV, current of 20 mA with Cu-Kα radiation of 1.541 Å. The data from the XRD machine were plotted using Origin 8.0 software to obtain full-width at half maximum (FWHM) value. The crystallite size of the nanoparticles was calculated using Scherrer's equation $D = 0.94 \lambda / \beta \cos \theta$ where D is the crystallite size, λ is the wavelength of the x-ray radiation, β denotes the FWHM value and θ is the angle of diffraction.

Transmission electron microscopy and selected area electron diffraction analysis

An aliquot of 10 µl of ethanolic colloidal solution of finely ground powder was drop-coated on a carbon-coated copper grid. This was then scanned using Philips-CM200 (Netherlands) TEM microscope operated at an accelerating voltage of 200 keV and selected area electron diffraction analysis was also carried out for the above-prepared sample. The size of the particles in the images was

measured and the mean value reported using the Image J software, USA.

Effect of SeNPs on the morphology of calcium oxalate crystals

Equal aliquots of an aqueous solution of 100 mmol L^{-1} sodium chloride, calcium chloride and sodium oxalate were mixed and filter sterilized to obtain a supersaturated solution of calcium oxalate according to method of Liang et al. (2009). Equal aliquots were then dispensed into three sterile beakers. A total of 50, 100 and $0 \mu\text{g ml}^{-1}$ SeNPs were added to the first, second and third beaker, respectively. A clean glass coverslip was then placed flat on the bottom of each beaker and the beakers kept standing at 37°C . After 3 days, the glass coverslips were removed from the beaker and dried at RT. The material on the glass coverslips was analysed by SEM-EDX, the crystal size measured and mean value reported using the Image J software, USA.

RESULTS

Growth and formation of selenium from selenite by *Hfx. alexandrinus* GUSF-1

Growth of the culture in selenite under aerobic conditions was accompanied by a visible reddish hue, turning to brick-red. In contrast, growth in the control flask without selenite was orange-red. Furthermore, the flask containing only medium and selenite, without the culture, did not exhibit any change in colour (Figure 1a). As the culture grew and more particulate matter was formed, monitoring of growth through absorbance at 600 nm was not possible since the particulate matter interfered in the measurement. Therefore, growth was determined by CFUs. *Hfx. alexandrinus* GUSF-1 grown in NTYE broth gave orange-red colonies (Figure 1b) while culture grown in NTYE broth with selenite gave brick-red colonies (Figure 1c). The absorption spectrum of acetone extract of the cells grown independent of selenite displayed peaks at 304 and 317 nm, two cis peaks at 368 and 386 nm, a broad shoulder

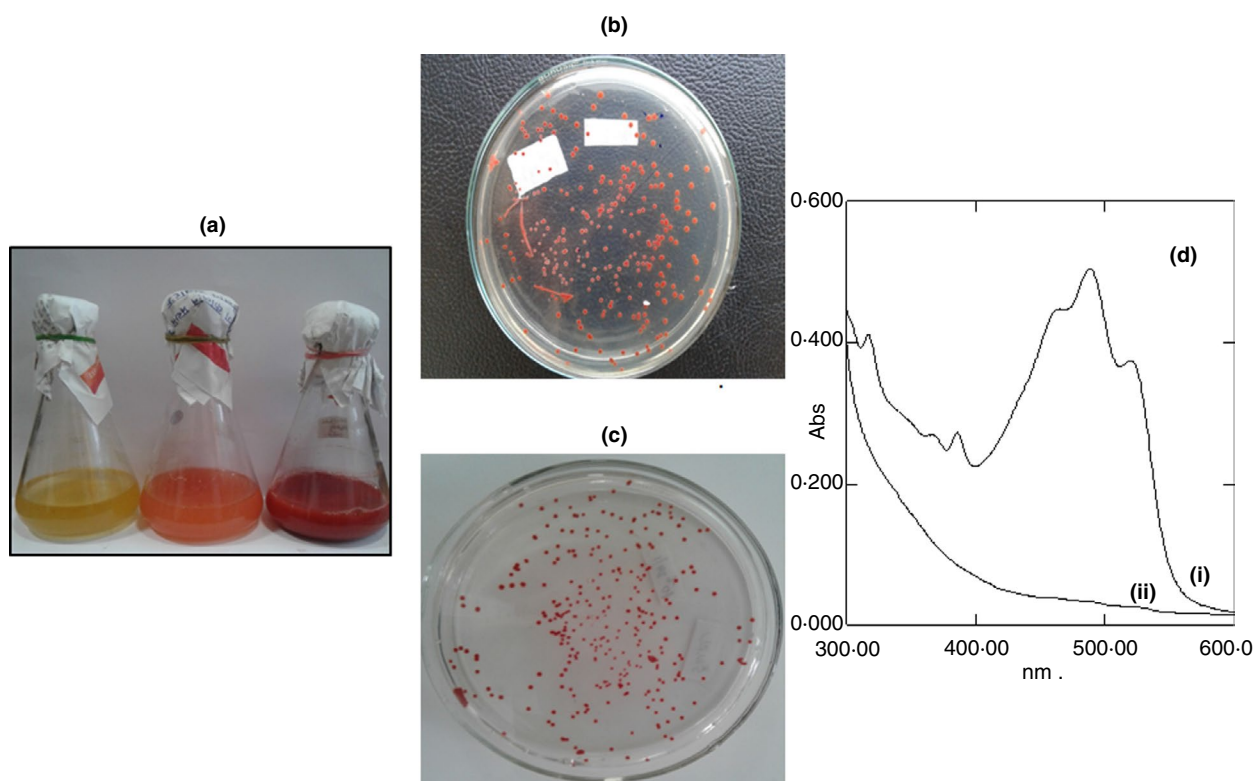


FIGURE 1 (a). Left: NaCl–tryptone–yeast extract (NTYE) with 5 mmol L^{-1} selenite (no colour change); centre: Growth of *Hfx. alexandrinus* GUSF-1 in NTYE (orange-red pigment formed); right: Growth of *Hfx. alexandrinus* GUSF-1 in NTYE in 5 mmol L^{-1} selenite (brick-red coloration) (b) Orange-red pigmented colonies of *Hfx. alexandrinus* GUSF-1 on NTYE solid agar (c) Brick-red colonies of *Hfx. alexandrinus* GUSF-1 on NTYE solid agar incorporated with 5 mmol L^{-1} selenite. Visible spectral scans of cellular pigment extracted with acetone on day 7 of growth from cells grown in (d(i)) NTYE depicting peaks at 304, 317, 368, 386, 463, 489 and 522 nm (extract is diluted with acetone $1:3 \text{ v v}^{-1}$) and (d(ii)) NTYE with 5 mmol L^{-1} selenite wherein the peaks have been abolished

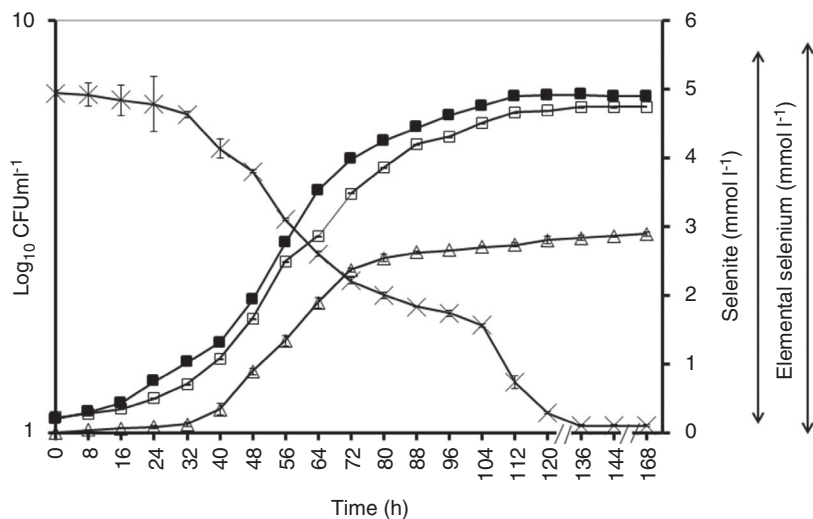


FIGURE 2 Time course of the growth of *Hfx. alexandrinus* GUSF-1 in the presence of 5 mmol L⁻¹ selenite. Growth monitored as Log₁₀ CFU ml⁻¹ in NaCl-tryptone-yeast extract (NTYE) (□) and in NTYE with 5 mmol L⁻¹ selenite (■); residual selenite (×) and formation of Se⁰ (Δ). The data shown is the mean of three replicates ± standard deviation (SD)

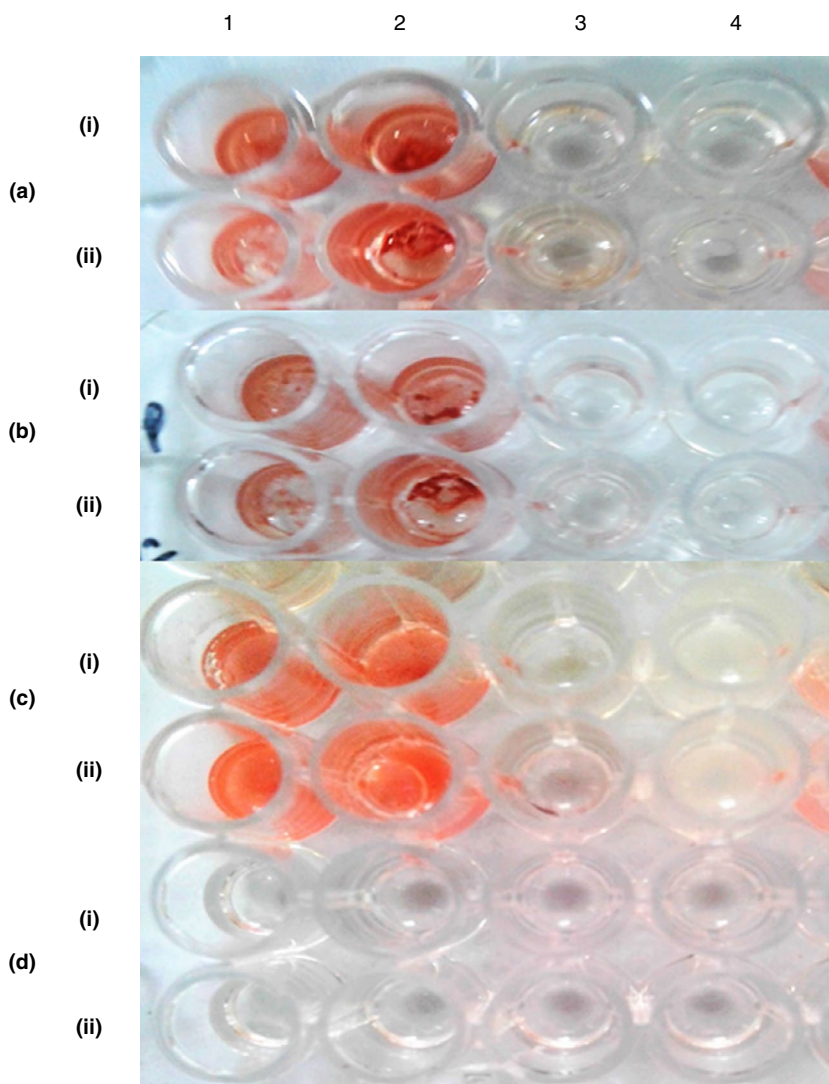
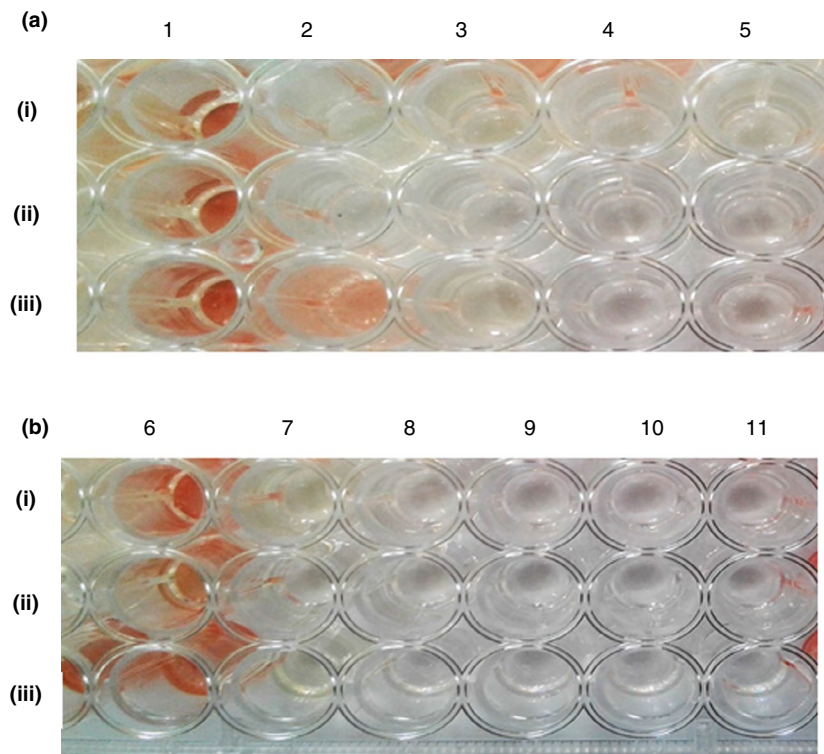


FIGURE 3 Conversion of 5 mmol L⁻¹ selenite using different fractions of *Hfx. alexandrinus* GUSF-1. (a) membrane fraction (MF) (b) soluble protein (SP) (c) cell-free supernatant (CFS) (d) extracellular polymeric substance (EPS). (i) buffer – pH 6 and (ii) buffer – pH 7; 1 and 2—two replicates of each fraction tested, 3—no selenite added, 4—no MF/SP/CFS/EPS

at 463 nm, and peaks at 489 and 522 nm, whereas no peaks were seen on the spectral scan of the acetone extract of cells grown in selenite (Figure 1d).

As shown in Figure 2, the presence of selenite did not drastically affect the final cell yield of *Hfx. alexandrinus* GUSF-1 and as compared to the culture growing without

FIGURE 4 Evaluation of enzyme inhibitors (a) sodium azide and (b) sodium arsenite on (i) membrane fraction (MF) (ii) soluble protein (SP) (iii) cell-free supernatant (CFS). 1 and 6 are the positive controls of MF/SP/CFS; 2 and 3 is 5 and 10 mmol L⁻¹ sodium azide; 7, 8 and 9 is 0.01, 0.05 and 0.1 mmol L⁻¹ sodium arsenite; 4 & 10—no selenite; 5 and 11—no MF/SP/CFS



selenite there was no difference in the lag phase. Growth approached the stationary phase faster, at 112 h in the presence of selenite, 24 h earlier than when grown without selenite. Selenite concentration steadily reduced up to 136 h of growth and was accompanied by strong garlic odour from 32 h onwards, which gradually diminished after 48 h. The formation of Se⁰ was indicated by the appearance of a faint red coloration from 40 h of growth, which steadily increased till 112 h. By the end of the stationary phase (168 h), 4.9 mmol L⁻¹ of selenite was reduced and the culture formed 2.89 mmol L⁻¹ of Se⁰.

CFS and cellular fractions, that is, SP and MF of *Hfx. alexandrinus* GUSF-1, formed selenium as observed in the micro-titre assay; the degree of brick-red particulate matter formed was MF > SP > CFS (Figure 3). This indicated that the active molecule/enzyme was located and active in SP (containing 120 µg of total protein) and also available in the MFs and the CFS. As demonstrated in Figure 4a, the formation of brick-red particulate matter by soluble protein and the membrane fraction was abolished by sodium azide at 5 and 10 mmol L⁻¹ concentrations, whereas 10 mmol L⁻¹ sodium azide was required to inhibit activity in CSF. All concentrations of sodium arsenite inhibited selenium formation in SP, MF and CSF visually to the same degree (Figure 4b).

Fourier-transform infrared spectrum

As seen in Figure 5a, the FT-IR spectrum of cells of *Hfx. alexandrinus* GUSF-1 grown in NTYE independent

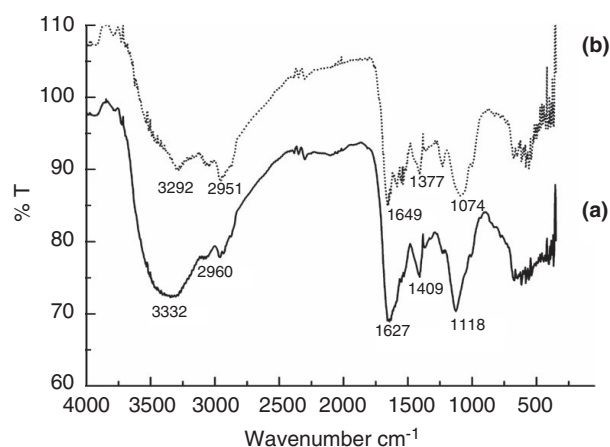


FIGURE 5 Fourier-transform infrared spectrum of cells of *Hfx. alexandrinus* GUSF-1 grown in (a) NaCl-tryptone-yeast extract (NTYE) and (b) NTYE + 5 mmol L⁻¹ selenite

of selenite showed peaks at 3332, 2960, 1627, 1409 and 1118 cm⁻¹. These peaks, however, as observed, were shifted to 3292, 2951, 1649, 1377 and 1074 cm⁻¹, respectively, in the presence of selenite (Figure 5b).

Characterization of SeNPs

The SEM micrograph of *Hfx. alexandrinus* GUSF-1 when grown in selenite (Figure 6a) showed the characteristic cup-shaped morphology, whereas the red particulate matter released from cells grown in selenite exhibited

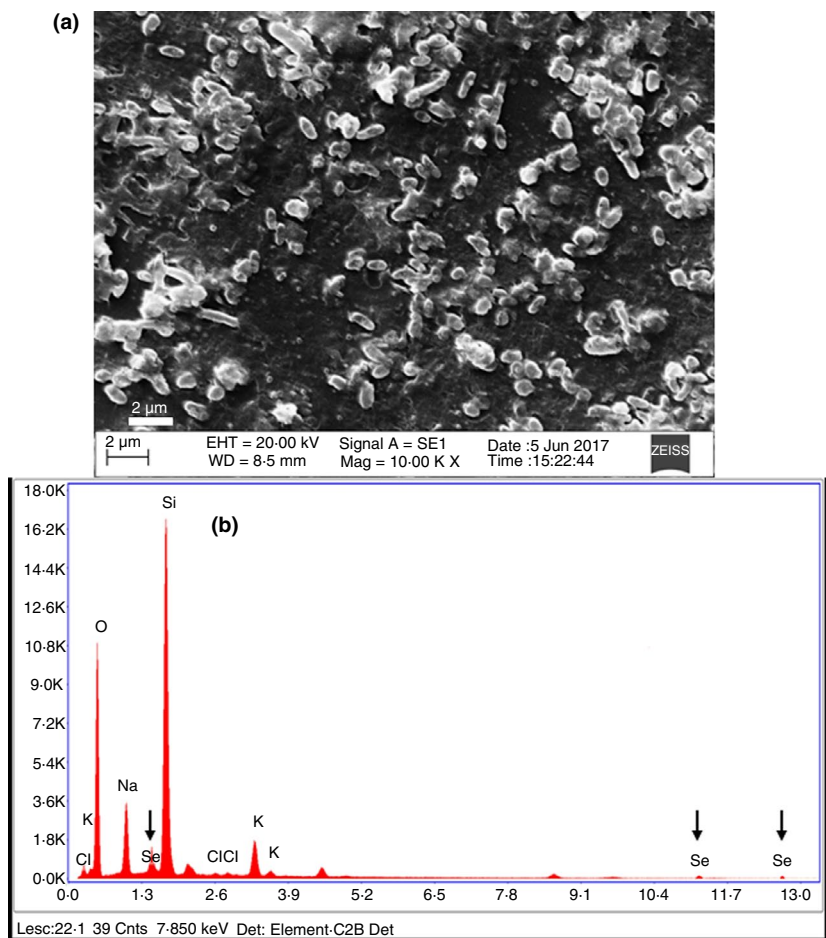


FIGURE 6 (a) SEM micrograph of cells of *Hfx. alexandrinus* GUSF-1 growing in the presence of 5 mmol L⁻¹ selenite (b) EDX micrograph of the purified brick-red material

absorption bands at 1.5, 11.2 and 12.5 keV in the EDX profile (Figure 6b) which confirmed the presence of Se⁰. Furthermore, Figure 7a revealed that the brick-red powder in methanol showed a characteristic peak at 239 nm in the UV absorption spectrum and an intensive peak at 254 cm⁻¹ in the Raman spectra (Figure 7b). The X-ray pattern of the brick-red powder depicted peaks corresponding to diffraction planes (100), (101), (110), (012), (111), (201), (112) and (022) at 2θ (degrees) of 23.40°, 29.66°, 41.26°, 43.68°, 45.24°, 51.62°, 55.93° and 61.47° with highest intensity at the (101) plane (Figure 8). The average crystallite size calculated using Scherrer's equation was 11.16 nm. The TEM imaging in Figure 9a,b exhibited pentagonal-shaped nanoparticles with an average diagonal length of 15 nm and a height of 50 nm. Furthermore, as depicted in Figure 9c, the selected area electron diffraction image exhibited diffraction rings corresponding to the (100), (101) and (012) directions of the hexagonal phase of selenium.

Effect of SeNPs in modulating the shape and size of calcium oxalate crystals

The EDX profile (Figure 10a) of calcium oxalate exhibited peaks for the presence of Ca, C and O. Calcium oxalate

crystals formed *in vitro* were rectangular with well-defined crystal borders and an average area of 1.23 ± 0.2 μm² was also observed. The presence of 50/100 μg ml⁻¹ of SeNPs affected the formation. The crystals formed in the presence of 50 μg ml⁻¹ SeNPs, were reduced in size, had an average area of 0.54 ± 0.2 μm² and irregular borders (Figure 10b). With the addition of 100 μg ml⁻¹ of SeNPs, the average area of the crystals was further decreased to 0.13 ± 0.005 μm² and the morphology changed to irregular spheres (Figure 10c). EDX analysis exhibited the presence of Ca, C and O and also confirmed the presence of Se⁰ with absorption bands at 1.5, 11.2 and 12.5 keV.

DISCUSSION

Microorganisms that live in niche environments are adapted to use more unusual substrates such as metal ions or chalcogen oxides. The reduction of these compounds results in the precipitation of insoluble products. Given this, the study focused on the interaction of an haloarchaeal isolate, *Hfx. alexandrinus* GUSF-1 (KF796625), with selenite. The formation of red colour, occurring during the growth of *Hfx. alexandrinus* GUSF-1 in the flask with selenite was attributed to the conversion of selenite

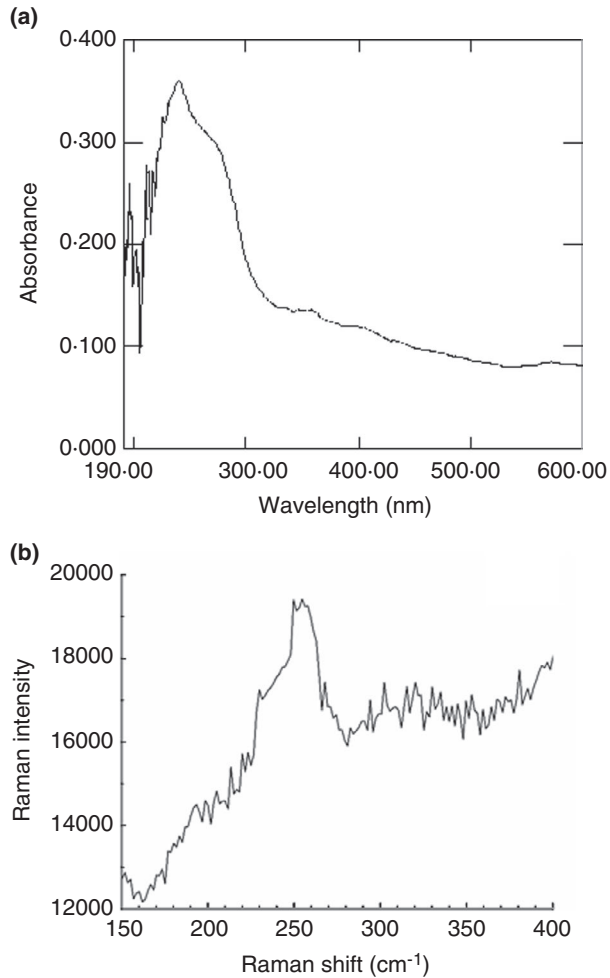
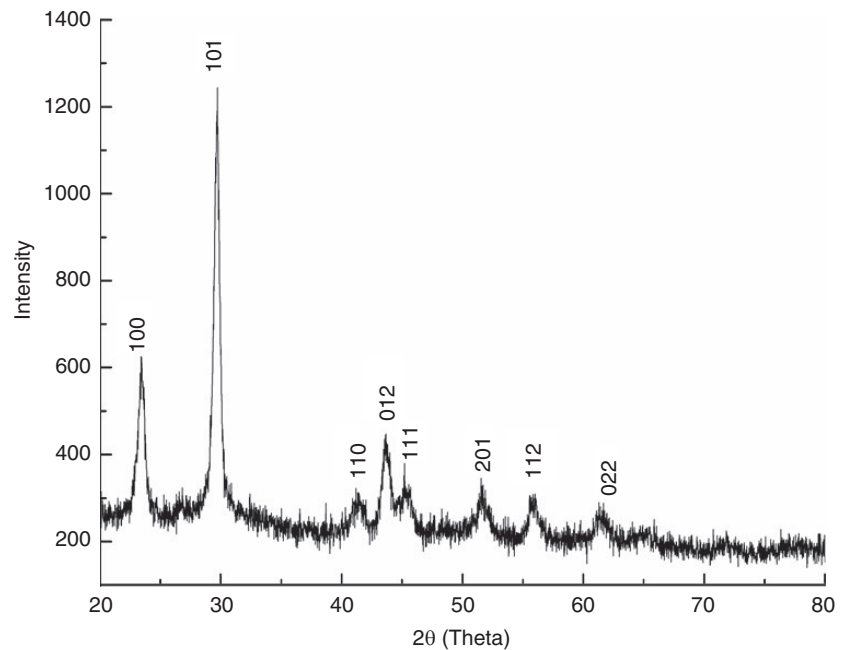


FIGURE 7 (a) UV-Vis spectrum and (b) Raman spectrum of SeNPs

FIGURE 8 X-ray diffraction profile of SeNPs



to Se^0 , also reported for bacteria (Khoie et al., 2017) and haloarchaea (Srivastava et al., 2014). According to Lampis et al. (2014), the development of such red-coloured particulate matter in the medium during the progression of growth of the culture occurs due to the reduction of selenite and is a characteristic of monoclinic colloidal Se^0 due to its surface plasmon excitation.

The visible absorption spectrum of the acetone extract of cells grown devoid of selenite showed the characteristic absorptions of red carotenoids consistent with the peaks reported for the C_{50} red carotenoid, bacterioruberin (Alvares & Furtado, 2021a). The presence of selenite in the medium during growth abolished all the peaks, suggesting the involvement of the pigment in formation of Se^0 from selenite. The cells of *Hfx. alexandrinus* GUSF-1 possess the full complement of pigment by the third day of growth and increases up to the seventh day which is available for interacting with selenite in medium and converting it to Se^0 , as discernible selenium was detected up to the seventh day of growth. This also confirmed that carotenoid biosynthesis was not affected by the presence of selenium, unlike that reported by Sams et al. (2011), for *Arabidopsis thaliana*, wherein selenium is argued to down-regulate phytoene synthase by selenium at the beginning of the carotenoid biosynthesis pathway.

The yield of the culture differed very slightly in the selenite supplemented medium compared with the growth in the control medium devoid of selenite. Plus, the lag phase between control and selenite growing culture was almost identical. This same behaviour in *R. rubrum* has been

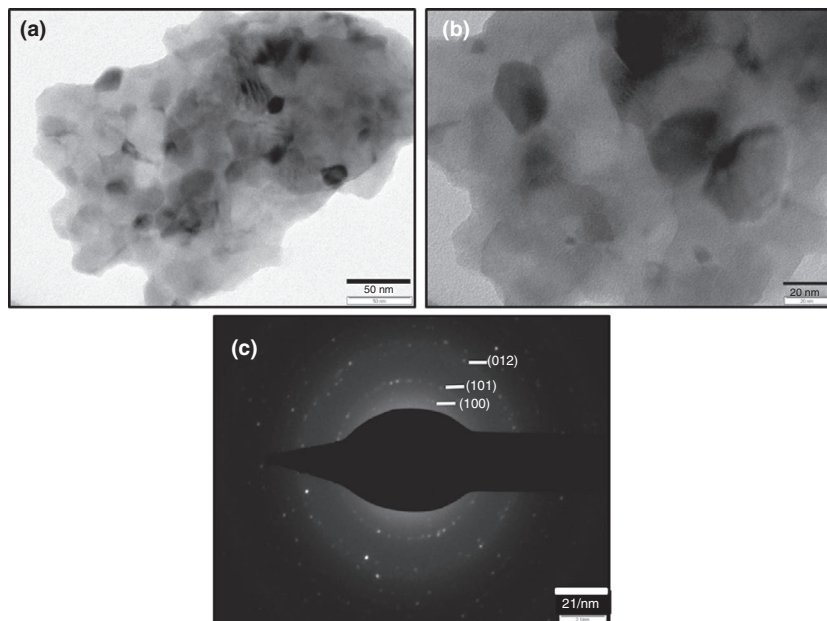


FIGURE 9 (a, b) TEM micrographs (different magnification) showing pentagonal-shaped nanoparticles (average diagonal length—15 nm and height—50 nm) and (c) selected area electron diffraction of SeNPs

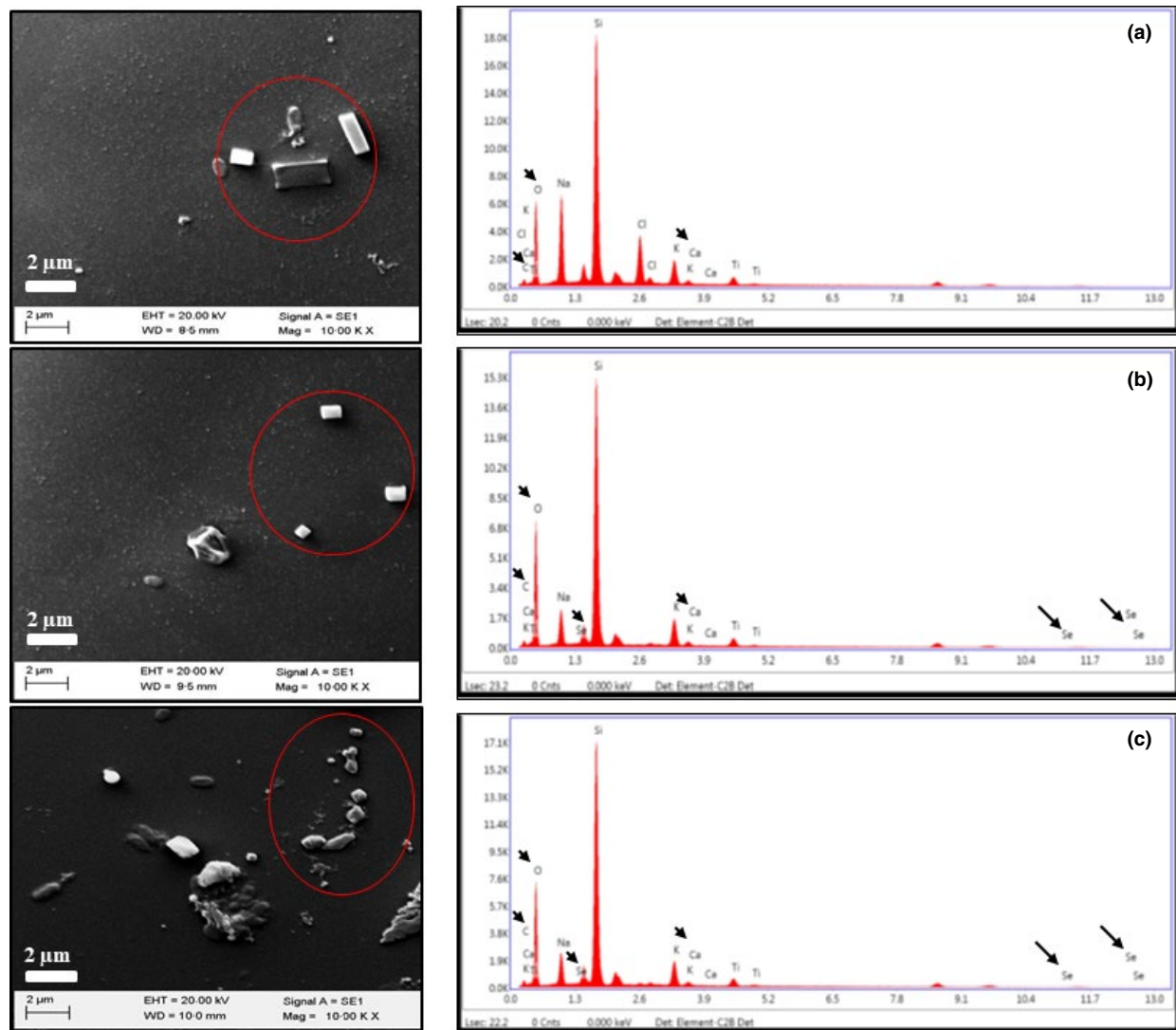


FIGURE 10 SEM analysis (left) and EDX profiles (right) of (a) calcium oxalate crystals; calcium oxalate crystals in the presence of (b) $50 \mu\text{g ml}^{-1}$ and (c) $100 \mu\text{g ml}^{-1}$ of SeNPs

reported by Kessi et al. (1999). This marginal difference in overall growth yield is attributed to the essential trace element property of selenium involved in the biosynthesis of selenocysteine, coenzyme Q and glutathione peroxidase (Navarro-Alarcón & López-Martínez, 2000). A remarkable clear garlic-like smell associated with growing cells cultured in the presence of selenite suggested the possible production of volatile organoselenium compounds which, according to Khoei et al. (2017), were also produced by strains of *Burkholderia fungorum* during growth in selenite. Production of volatile selenium compounds has also been reported in *R. sphaeroides* (Van Fleet-Stalder et al., 2000) and in a euryhaline green microalga species of *Chlorella*, which aerobically transforms selenite into a variety of volatile Se compounds (Fan et al., 1997). A decrease in selenite concentration was seen from the beginning of the exponential phase (32 h). The increase from selenite to Se^0 progressed, concomitantly with the increase in cell growth, and corroborated with results reported for selenite reduction by Lampis et al. (2014), during the growth of *Bacillus mycoides* SeITE01 in the presence of selenite. This formation of Se^0 continued till stationary phase (112 h), similar to selenite reduction that is reported in the haloarchaeon *H. salifonidae* BK18 (Srivastava et al., 2014) and observed in *B. fungorum* DBT1 (Khoei et al., 2017). Unlike results obtained in this study, selenite reduction is shown to occur between the end of the exponential phase and the beginning of the stationary phase in *Rhodospseudomonas palustris* strain N and *R. rubrum* by Li et al. (2014) and Kessi et al. (1999). Furthermore, delayed formation of Se^0 (from 40 h) in spite of the progress in decrease in selenite, reflects that the culture assimilates the selenium formed in the initial growth phase, which is lost as volatile intermediates. A similar delay is seen in *B. mycoides* SeITE01 by Lampis et al., 2014. *Hfx. alexandrinus* GUSF-1 yielded 2.89 mmol L^{-1} of Se^0 in 168 h of growth in selenite; this low yield of Se^0 together with the observation of garlic-like odour points to the formation of volatile compounds (not yet confirmed) in addition to Se^0 . Future investigations dedicated to unveiling the detailed mechanism of interaction between *Hfx. alexandrinus* GUSF-1 and selenite are warranted.

The inhibition of the formation of red Se^0 particulate matter on the addition of sodium azide to selenite and SP/MF/CFS indicated that the transformation of selenite to Se^0 was arrested. Inhibition of selenite reduction by sodium azide is reported in the haloarchaeon *Halococcus salifodinae* BK18 (Srivastava et al., 2014). Haloarchaeal proteins and enzymes are expected to disintegrate in aqueous, that is, high water activity (a_w). We, however, observed that lysing *Hfx. alexandrinus* GUSF-1 cells by suspending them in water to a volume less than the volume of culture broth used for harvesting cells and using the

lysate instantly exhibited formation of red Se^0 precipitate to a degree, visually discernible. Similarly, the formation of Se^0 was stopped in the presence of sodium arsenite. At this point of time and with limited basic results, it is appropriate to conclude that some of the biomolecules involved in conversion of selenite to Se^0 are Fe containing. The CFS had 25% NaCl; MF was suspended in 15% NaCl; and the SP was in aqueous lysate, the question therefore arises, how were the proteins and enzymes active? To our understanding *Hfx. alexandrinus* GUSF-1 exposed to just enough water to lyse the cells and the lysates examined instantly for the ability to convert selenite to Se^0 , approximately had 1.712 M NaCl, besides other salts such as MgCl_2 and KCl, which guarded the integrity of SPs and other molecules present. Hence, the reason for the portrayed activity in the micro-titre plates. We, however, suggest that *Hfx. alexandrinus* GUSF-1 may be using enzymes, which to our surprise remain active at 1.712 M NaCl to a degree, this significant feature is under investigation. As lysates of *Hfx. alexandrinus* GUSF-1 cells invariably possess C_{50} pigment bacterioruberin that are active antioxidants (Alvares & Furtado, 2021a), we conclude the involvement of bacterioruberin in the formation of Se^0 from selenite, which is also supported by its decline during growth *Hfx. alexandrinus* GUSF-1 in selenite, possibly because of its interaction with selenite. Besides, other proteins/enzymes, which are affected by the presence of sodium azide and sodium arsenite could also be involved in the conversion process.

Furthermore, the FTIR results clearly showed and confirmed the presence of biomacromolecules that might have participated in the biotransformation process or remain absorbed to the Se^0 particles during the release of selenium from cells and now would act as capping agents. Tugarova et al. (2018) also reported the presence of organic capping material on SeNPs biosynthesized by bacterium *Azospirillum thiophilum*. The shift in the FTIR peaks is also reported by Patil et al. (2014) for this same culture during its interaction with silver nitrate and its subsequent reduction to silver nanoparticles. Broad peaks in $3332/3292 \text{ cm}^{-1}$ arose due to the stretching of the N-H bonds of amine (-NH) groups and the O-H bonds of the hydroxyl (-OH) groups. The absorption peaks at $2960/2951 \text{ cm}^{-1}$ were because of the asymmetric stretching and bending vibrations of the C-H bond of the $-\text{CH}_2$ groups combined with that of the CH_3 groups. The peak at $1627/1649 \text{ cm}^{-1}$ is attributed to amide I (in proteins). The peak at $1409/1377 \text{ cm}^{-1}$ corresponding to the skeletal vibrations of $-\text{CH}_2-$, $-\text{CH}_3-$, $-\text{OH}$, C-C, C-O, C-O-C groups. The absorption at $1118/1074 \text{ cm}^{-1}$ was typical of functional groups arising from polysaccharides.

The elemental composition as reported by the EDX analysis was consistent with that reported by Lampis

et al. (2014) and Srivastava et al. (2014). The red particulate matter showed a characteristic UV absorption peak at 240 nm, fairly close to 248 nm reported for SeNPs synthesized by *Klebsiella pneumoniae* (Fesharaki et al., 2010). *H. salifodinae* BK18 produced SeNPs with absorption at 270 nm (Srivastava et al., 2014). The peak at 254 cm⁻¹ detected in the Raman spectrum was also in line with that reported by Mateleshko et al. (2004) for crystalline selenium. Furthermore, the XRD pattern revealed the formation of monophasic hexagonal selenium without any traces of impurity phases and matched the JCPDS card no. 073-0465 and also supported the results of Raman spectra. Additionally, TEM images supported a pentagonal morphology. A mixture of different forms of SeNPs are reported from cultures across other domains of life, such as polygonal using extracts of *Capsicum annuum* L (Li et al., 2007), rods by *Streptomyces bikiniensis* strain Ess_ama-1 (Ahmad et al., 2015) and by the haloarchaeon, *H. salifodinae* BK18 (Srivastava et al., 2014). Though Se⁰ biosynthesized by bacteria are primarily spherical and in the range of 20–500 nm (Wadhvani et al., 2016), this is the first report of pentagonal SeNPs in haloarchaea. Biogenically produced SeNPs are known to possess various significant biomedical applications (Prasad et al., 2013; Prasad & Selvaraj, 2014; Srivastava et al., 2014). The presence of SeNPs biosynthesized by the culture *Hfx. alexandrinus* GUSF-1 modulated *in vitro*, the formation of shape and size of calcium oxalate monohydrate to smaller rectangular and irregular spherical forms as evident in SEM-EDX profiles, with peaks for the elemental components of Ca, C, O calcium oxalate and the added SeNPs.

Modulation of calcium oxalate crystals during formation is reported using nano selenium concentration different from that used in this study. Besides, the nanoselenium used in their study was synthesized using chemical reduction of selenious dioxide with ascorbic acid and also using leaf extract of *Ocimum tenuiflorum*. For example, Liang et al., 2009 and Liang et al., 2020 reported the modulation using 2.3 µg ml⁻¹ of nanoselenium while a similar modulation of size and shape was achieved using 22 µg ml⁻¹ (Zhong et al., 2015). The use of urolithiatic molecules such as phytic acid and chit molecules conjugated with gallic acid (Chit-Gal) are reported for treatment of urolithiasis but limited due to the expensive synthesis involved (Ahmed et al., 2016; Queiroz et al., 2019). Hence, SeNPs, which are known to exhibit low cytotoxicity, possess antioxidant property and reported to enhance the efficacy of selenoenzymes in mammalian biology (Wang et al., 2007) according to us, holds a promise in treatment that is cost-effective.

In this study, the ability of *Hfx. alexandrinus* GUSF-1 (KF796625) to grow and convert selenite was investigated. The culture achieved conversion efficiency of 98% and 2.89 mmol L⁻¹ of Se⁰ was formed at the end of 168 h.

Reports on conversion of selenite reduction in extreme halophiles are rare, with no reports among *Haloferax* genera, and this study involving the formation of pentagonal selenium nanoparticles in haloarchaea is recorded as the first report. This *in vitro* study also clearly demonstrated the ability of these nanoparticles to successfully modulate the rectangular shape and size of calcium oxalate crystals and hence is of importance in pharmaceutical formulation for abetting urinary calculi. Furthermore, we recommend using haloarchaea for the biosynthesis of nanomaterial, as NaCl/high salt requirement for culturing ensures an aseptic environment, minimizing the cost of culturing, thus providing an economically viable green synthesis route.

ACKNOWLEDGEMENTS

The authors thank the following institutes for the different facilities provided: Indian Institute of Technology-Bombay, for TEM, Malaviya National Institute of Technology Jaipur for Raman Spectroscopy, National Institute of Oceanography, Goa for the XRD profiling, University Science Instrumentation Centre (USIC) for SEM-EDX and Department of Chemistry, Goa University for FT-IR analysis.

CONFLICT OF INTEREST

The authors declare that they have no conflict of interest.

ORCID

Irene J. Furtado  <https://orcid.org/0000-0002-7619-6340>

REFERENCES

- Abdollahnia, M., Makhdomi, A., Mashreghi, M. & Eshghi, H. (2020) Exploring the potentials of halophilic prokaryotes from a solar saltern for synthesizing nanoparticles: the case of silver and selenium. *PLoS ONE*, 15(3), e0229886. <https://doi.org/10.1371/journal.pone.0229886>
- Ahmad, M.S., Yasser, M.M., Sholkamy, E.N., Ali, A.M. & Mehanni, M.M. (2015) Anticancer activity of biostabilized selenium nanorods synthesized by *Streptomyces bikiniensis* strain Ess_ama-1. *International Journal of Nanomedicine*, 10, 3389–3401. <https://doi.org/10.2147/IJN.S82707>
- Ahmed, S., Hasan, M.M. & Mahmood, Z.A. (2016) Inhibition and modulation of calcium oxalate monohydrate crystals by phytic acid: an *in vitro* study. *Journal of Pharmacognosy and Phytochemistry*, 5(2), 91–95.
- Alvares, J.J. & Furtado, I.J. (2018) Extremely halophilic Archaea and Eubacteria are responsible for free radical scavenging activity of solar salts of Goa-India. *Global Journal of Bio-science and Biotechnology*, 7(2), 242–254.
- Alvares, J.J. & Furtado, I.J. (2021a) Characterization of multicomponent antioxidants from *Haloferax alexandrinus* GUSF-1 (KF796625). 3. *Biotech*, 11(2), 58. <https://doi.org/10.1007/s13205-020-02584-9>
- Alvares, J.J. & Furtado, I.J. (2021b) Anti-*Pseudomonas aeruginosa* biofilm activity of tellurium nanorods biosynthesized

- by cell lysate of *Haloferax alexandrinus* GUSF-1(KF796625). *BioMetals*, 34(5), 1007–1016. <https://doi.org/10.1007/s10534-021-00323-y>
- Alvares, J.J. & Furtado, I.J. (2021c) Kinetics of DPPH• scavenging by bacterioruberin from *Haloferax alexandrinus* GUSF-1 (KF796625). *Journal of Analytical Science and Technology*, 12, 44. <https://doi.org/10.1186/s40543-021-00293-3>.
- Barnaby, S.N., Frayne, S.H., Fath, K.R. & Banerjee, I.A. (2011) Growth of Se nanoparticles on kinetin assemblies and their biocompatibility studies. *Soft Materials*, 9, 313–334. <https://doi.org/10.1080/1539445X.2010.516302>
- Bebien, M., Chauvin, J.P., Adriano, J.M., Grosse, S. & Verméglio, A. (2001) Effect of selenite on growth and protein synthesis in the phototrophic bacterium *Rhodobacter sphaeroides*. *Applied and Environment Microbiology*, 67(10), 4440–4447. <https://doi.org/10.1128/AEM.67.10.4440-4447.2001>
- Biswas, K.C., Barton, L.L., Tsui, W.L., Shuman, K., Gillespie, J. & Eze, C.S. (2011) A novel method for the measurement of elemental selenium produced by bacterial reduction of selenite. *Journal of Microbiol Methods*, 86(2), 140–144. <https://doi.org/10.1016/j.mimet.2011.04.009>
- Debieux, C.M., Dridge, E.J., Mueller, C.M., Splatt, P., Paszkiewicz, K., Knight, I. et al. (2011) A bacterial process for selenium nanosphere assembly. *Proceedings of the National Academy of Sciences of the United State of America*, 108(33), 13480–13845. <https://doi.org/10.1073/pnas.1105959108>
- Del Gallo, M. & Haegi, A. (1990) Characterization and quantification of exocellular polysaccharides in *Azospirillum brasilense* and *Azospirillum lipoferum*. *Symbiosis*, 9, 155–161.
- DeMoll-Decker, H. & Macy, J.M. (1993) The periplasmic nitrite reductase of *Thauera selenatis* may catalyze the reduction of selenite to elemental selenium. *Archives of Microbiology*, 160, 241–247. <https://doi.org/10.1007/BF00249131>
- Fan, T.-W.-M., Lane, A.N. & Higashi, R.M. (1997) Selenium biotransformations by a euryhaline microalga isolated from a saline evaporation pond. *Environmental Science and Technology*, 31(2), 569–576.
- Fesharaki, P.J., Nazari, P., Shakibaie, M., Rezaie, S., Banoee, M., Abdollahi, M. et al. (2010) Biosynthesis of selenium nanoparticles using *Klebsiella pneumoniae* and their recovery by a simple sterilization process. *Brazilian Journal of Microbiology*, 41(2), 461–466.
- Forootanfar, H., Zare, B., Fasihi-Bam, H., Amirpour-Rostami, S., Ameri, A., Shakibaie, M. et al. (2013) Biosynthesis and characterization of selenium nanoparticles produced by terrestrial actinomycete *Streptomyces microflavus* strain FSHJ31. *Research and Reviews: Journal of Microbiology and Biotechnology*, 3, 47–53.
- Ganther, H.E. (1971) Reduction of the selenotrisulfide derivative of glutathione to a persulfide analog by glutathione reductase. *Biochemistry*, 10(22), 4089–4098. <https://doi.org/10.1021/bi00798a013>
- Gaonkar, S.K. & Furtado, I.J. (2018) Isolation and culturing of protease- and lipase-producing *Halococcus agarilyticus* GUGFAWS-3 from marine *Haliclona* sp. inhabiting the rocky intertidal region of Anjuna in Goa, India. *Annals of Microbiology*, 68, 851–861. <https://doi.org/10.1007/s13213-018-1391-6>
- Gharieb, M.M., Wilkinson, S.C. & Gadd, G.M. (1995) Reduction of selenium oxyanions by unicellular, polymorphic and filamentous fungi: cellular location of reduced selenium and implications for tolerance. *Journal of Industrial Microbiology*, 14, 300–311.
- Güven, K., Mutlu, M.B., Çırpan, C. & Kutlu, H.M. (2013) Isolation and identification of selenite reducing archaea from Tuz (salt) Lake In Turkey. *Journal of Basic Microbiology*, 53(5), 397–401. <https://doi.org/10.1002/jobm.201200008>
- Institute of Medicine (US) Panel on Dietary Antioxidants and Related Compounds. (2000) Dietary reference intakes for vitamin C, vitamin E, selenium, and carotenoids, 7, Selenium. Washington, DC: National Academies Press (US). Available at: <https://www.ncbi.nlm.nih.gov/books/NBK225470>
- Kessi, J. & Hanselmann, K.W. (2004) Similarities between the abiotic reduction of selenite with glutathione and the dissimilatory reaction mediated by *Rhodospirillum rubrum* and *Escherichia coli*. *Journal of Biological Chemistry*, 279(49), 50662–50669.
- Kessi, J., Ramuz, M., Wehrli, E., Spycher, M. & Bachofen, R. (1999) Reduction of selenite and detoxification of elemental selenium by the phototrophic bacterium *Rhodospirillum rubrum*. *Applied and Environment Microbiology*, 65(11), 4734–4740. <https://doi.org/10.1128/AEM.65.11.4734-4740.1999>
- Khoei, N.S., Lampis, S., Zonaro, E., Yrjälä, K., Bernardi, P. & Vallini, G. (2017) Insights into selenite reduction and biogenesis of elemental selenium nanoparticles by two environmental isolates of *Burkholderia fungorum*. *New Biotechnology*, 34, 1–11. <https://doi.org/10.1016/j.nbt.2016.10.002>
- Klonowska, A., Heulin, T. & Verméglio, A. (2005) Selenite and tellurite reduction by *Shewanella oneidensis*. *Applied and Environment Microbiology*, 71(9), 5607–5609. <https://doi.org/10.1128/AEM.71.9.5607-5609.2005>
- Lampis, S., Zonaro, E., Bertolini, C., Bernardi, P., Butler, C.S. & Vallini, G. (2014) Delayed formation of zero-valent selenium nanoparticles by *Bacillus mycoides* SeITE01 as a consequence of selenite reduction under aerobic conditions. *Microbial Cell Factories*, 13(1), 35.
- Li, B., Liu, N.A., Li, Y., Jing, W., Fan, J., Li, D. et al. (2014) Reduction of selenite to red elemental selenium by *Rhodospseudomonas palustris* Strain N. *PLoS One*, 9(4), e95955. <https://doi.org/10.1371/journal.pone.0095955>
- Li, S., Shen, Y., Xie, A., Yu, X., Zhang, X., Yang, L. et al. (2007) Rapid, room temperature synthesis of amorphous selenium/protein composites using *Capsicum annuum* L extract. *Nanotechnology*, 18, 405101. <https://doi.org/10.1088/0957-4484/18/40/405101>
- Liang, M., Bai, Y., Huang, L., Zheng, W. & Liu, J. (2009) Inhibition of the crystal growth and aggregation of calcium oxalate by elemental selenium nanoparticles. *Colloids and Surfaces B: Biointerfaces*, 74(1), 366–369. <https://doi.org/10.1016/j.colsurfb.2009.07.038>
- Liang, T., Qiu, X., Ye, X., Liu, Y., Li, Z., Tian, B. et al. (2020) Biosynthesis of selenium nanoparticles and their effect on changes in urinary nanocrystallites in calcium oxalate stone formation. *3 Biotech*, 10(1), 23. <https://doi.org/10.1007/s1320-5-019-1999-7>
- Lieske, J.C., Deganello, S. & Toback, F.G. (1999) Cell-crystal interactions and kidney stone formation. *Nephron*, 81(suppl 1), 8–17. <https://doi.org/10.1159/000046293>
- Losi, M.E. & Frankenberger, W.T. (1997) Reduction of selenium oxyanions by *Enterobacter cloacae* SLD1a-1: isolation and growth of the bacterium and its expulsion of selenium particles. *Applied and Environment Microbiology*, 63, 3079–3084.

- Lowry, O.H., Rosebrough, N.J., Farr, A.L. & Randall, R.J. (1951) Protein measurement with the Folin phenol reagent. *Journal of Biological Chemistry*, 193, 265–275.
- Lulich, J.P., Osborne, C.A., Carvalho, M. & Nakagawa, Y. (2012) Effects of a urolith prevention diet on urine compositions of glycosaminoglycans, Tamm-Horsfall glycoprotein, and nephrocalcin in cats with calcium oxalate urolithiasis. *American Journal of Veterinary Research*, 73(3), 447–451. <https://doi.org/10.2460/ajvr.73.3.447>
- Luo, L.B., Jie, J.S., Chen, Z.H., Zhang, X.J., Fan, X., Yuan, G.D. et al. (2009) Photoconductive properties of selenium nanowire photodetectors. *Journal of Nanoscience and Nanotechnology*, 9(11), 6292–6298. <https://doi.org/10.1166/jnn.2009.1468>
- Macy, J.M., Lawson, S. & DeMoll-Decker, H. (1993) Bioremediation of selenium oxyanions in San Joaquin drainage water using *Thauera selenatis* in a biological reactor system. *Applied Microbiology and Biotechnology*, 40, 588–594.
- Malhotra, S., Jha, N. & Desai, K. (2014) A superficial synthesis of selenium nanospheres using wet chemical approach. *International Journal of Nanotechnology and Application*, 3(4), 7–14.
- Mateleshko, N., Mitsa, V., Veres, M. & Koos, M. (2004) Investigation of nanophase separation in Glassy As₄₀Se₆₀ using Raman scattering and AB initio calculations. *Chalcogenide Letters*, 1(11), 139–144.
- Naik, S. & Furtado, I. (2019) Formation of Rhodochrosite by *Haloferax alexandrinus* GUSF-1. *Journal of Cluster Science*, 30, 1435–1441. <https://doi.org/10.1007/s10876-019-01586-9>
- Navarro-Alarcón, M. & López-Martínez, M.C. (2000) Essentiality of selenium in the human body: relationship with different diseases. *Science of the Total Environment*, 249(1–3), 347–371. [https://doi.org/10.1016/S0048-9697\(99\)00526-4](https://doi.org/10.1016/S0048-9697(99)00526-4)
- Papp, L.V., Lu, J., Holmgren, A. & Khanna, K.K. (2007) From selenium to selenoproteins: synthesis, identity, and their role in human health. *Antioxidants & Redox Signaling*, 9(7), 775–806. <https://doi.org/10.1089/ars.2007.1528>
- Patil, S., Fernandes, J., Tangsali, R.B. & Furtado, I.J. (2014) Exploitation of *Haloferax alexandrinus* for biogenic synthesis of silver nanoparticles antagonistic to human and lower mammalian pathogens. *Journal of Cluster Science*, 25, 423–433. <https://doi.org/10.1007/s10876-013-0621-0>
- Prasad, K.S., Patel, H., Patel, T., Patel, K. & Selvaraj, K. (2013) Biosynthesis of Se nanoparticles and its effect on UV-induced DNA damage. *Colloids and Surfaces B: Biointerfaces*, 103, 261–266. <https://doi.org/10.1016/j.colsurfb.2012.10.029>
- Prasad, K.S. & Selvaraj, K. (2014) Biogenic synthesis of selenium nanoparticles and their effect on As(III)-induced toxicity on human lymphocytes. *Biological Trace Element Research*, 157(3), 275–283. <https://doi.org/10.1007/s12011-014-9891-0>
- Queiroz, M.F., Melo, K.R.T., Sabry, D.A., Sasaki, G.L., Rocha, H.A.O. & Costa, L.S. (2019) Gallic acid-chitosan conjugate inhibits the formation of calcium oxalate crystals. *Molecules*, 24(11), 2074. <https://doi.org/10.3390/molecules24112074>
- Raghavan, T.M. & Furtado, I. (2004) Occurrence of extremely halophilic Archaea in sediments from the continental shelf of west coast of India. *Current Science*, 86(8), 1065–1067.
- Sams, C.E., Panthee, D.R., Charron, C.S., Kopsell, D.A. & Yuan, J.S. (2011) Selenium regulates gene expression for glucosinolate and carotenoid biosynthesis in *Arabidopsis*. *Journal of the American Society for Horticultural Science*, 136(1), 23–34. <https://doi.org/10.21273/JASHS.136.1.23>
- Sequeira, F. (1992) Microbiological study of salt pans of Goa. M.Sc. dissertation thesis. Goa University, India.
- Sharma, G., Sharma, A.R., Bhavesh, R., Park, J., Ganbold, B., Nam, J.-S. et al. (2014) Biomolecule-mediated synthesis of selenium nanoparticles using dried *Vitis vinifera* (raisin) extract. *Molecules*, 19(3), 2761–2770. <https://doi.org/10.3390/molecules19032761>
- Srivastava, P., Bragança, J.M. & Kowshik, M. (2014) *In vivo* synthesis of selenium nanoparticles by *Halococcus salifodinae* BK18 and their anti-proliferative properties against HeLa cell line. *Biotechnology Progress*, 30(6), 1480–1487. <https://doi.org/10.1002/btpr.1992>
- Tugarova, A.V., Mamchenkova, P.V., Dyatlova, Y.A. & Kamnev, A.A. (2018) FTIR and Raman spectroscopic studies of selenium nanoparticles synthesised by the bacterium *Azospirillum thioophilum*. *Spectrochimica Acta Part A: Molecular and Biomolecular Spectroscopy*, 192, 458–463. <https://doi.org/10.1016/j.saa.2017.11.050>
- Van Fleet-Stalder, V., Chasteen, T.G., Pickering, I.J., George, G.N. & Prince, R.C. (2000) Fate of selenate and selenite metabolized by *Rhodobacter sphaeroides*. *Applied and Environment Microbiology*, 66(11), 4849–4853. <https://doi.org/10.1128/AEM.66.11.4849-4853.2000>
- Wadhvani, S.A., Shedbalkar, U.U., Singh, R. & Chopade, B.A. (2016) Biogenic selenium nanoparticles: current status and future prospects. *Applied Microbiology and Biotechnology*, 100(6), 2555–2566. <https://doi.org/10.1007/s00253-016-7300-7>
- Wang, H., Zhang, J. & Yu, H. (2007) Elemental selenium at nano size possesses lower toxicity without compromising the fundamental effect on selenoenzymes: comparison with selenomethionine in mice. *Free Radical Biology and Medicine*, 42(10), 1524–1533. <https://doi.org/10.1016/j.freeradbiomed.2007.02.013>
- Wen, H. & Carignan, J. (2007) Reviews on atmospheric selenium: emissions, speciation and fate. *Atmospheric Environment*, 41(34), 7151–7165. <https://doi.org/10.1016/j.atmosenv.2007.07.035>
- Zhang, J. & Spallholz, J.E. (2011) Toxicity of selenium compounds and nano-selenium particles. *General, Applied Systems Toxicology*. <https://doi.org/10.1002/9780470744307.gat243>
- Zhong, C., Deng, Z., Wang, R. & Bai, Y. (2015) Inhibition mechanism of calcium oxalate crystal growth by cooperation influence of colloidal selenium nanoparticles and bovine serum albumin. *Crystal Growth & Design*, 15(4), 1602–1610. <https://doi.org/10.1021/cg500880m>

How to cite this article: Alvares, J.J. & Furtado, I.J. (2021) Conversion of selenite by *Haloferax alexandrinus* GUSF-1 (KF796625) to pentagonal selenium nanoforms which in vitro modulates the formation of calcium oxalate crystals. *Journal of Applied Microbiology*, 00, 1–14. <https://doi.org/10.1111/jam.15309>